

Efficient Ligand Passivation Enables Ultrastable CsPbX₃ Perovskite Nanocrystals in Fully Alcohol Environments

Andrés F. Gualdrón-Reyes,* Roser Fernández-Climent, Sofia Masi, Camilo A. Mesa, Carlos Echeverría-Arrondo, Federica Aiello, Federica Balzano, Gloria Uccello-Barretta, Jhonatan Rodríguez-Pereira, Sixto Giménez, and Iván Mora-Seró*

Halide perovskite nanocrystals (PNCs) have demonstrated their wide potential to fabricate efficient optoelectronic devices and to prepare promising photocatalysts for solar-driven photo(electro)chemical reactions. However, their use in most of the practical applications is limited due to the instability of PNCs in polar environments. Here, the preparation of non-encapsulated CsPbX₃ nanocrystals dispersed in fully alcohol environments, with outstanding stability through surface defect passivation strategy is reported. By using didodecyldimethylammonium bromide (DDAB) during material post-treatment, highly luminescent CsPbBr₃ PNCs with remarkable stability in methanol/butanol medium up to 7 months with near-unity photoluminescence quantum yield are achieved. This approach is extrapolated to stabilize iodine-based CsPbBr_{3-x}I_x and CsPbI₃ PNCs, showing an improvement of their photoluminescence features and stability in these high polar alcohols up to 6 h. DDAB mediates the defect suppression through ligand exchange and avoids the full permeation of alcohol to be in contact with the PNCs. In this context, DDAB induces ionization of alcohol molecules to strengthen the surface passivation. The findings open the door to the development of long-term stable CsPbX₃ PNCs with high optical performance to be used in polar environments.

1. Introduction

Since their first appearance in 2014, halide perovskite nanocrystals (PNCs) have revolutionized the fields of optoelectronics and photovoltaics, due to their outstanding photophysical and electronic properties.^[1,2] These materials have a labile structure to dictate their optical features such as the band gap,^[3] high absorption coefficient,^[4] improved carrier transport ability,^[5] versatile synthetic pathways,^[6,7] low-production costs and impressive tolerance to defects (with near-unity photoluminescence quantum yield, PLQY).^[8,9] These fascinating properties have guaranteed the success to achieve relevant breakthroughs such as the fabrication of highly efficient light-emitting diodes with external quantum efficiencies >20%^[10–12] and PNCs-based solar cells reaching closer values to the records of bulk-based ones.^[13,14] Certainly, their capability to capture solar energy and store it through the

A. F. Gualdrón-Reyes, R. Fernández-Climent, S. Masi, C. A. Mesa, C. Echeverría-Arrondo, S. Giménez, I. Mora-Seró
Institute of Advanced Materials (INAM), Universitat Jaume I (UJI),
Avenida de Vicent Sos Baynat, s/n
Castelló de la Plana
Castellón 12071, Spain
E-mail: andres.gualdron@uach.cl; sero@uji.es


A. F. Gualdrón-Reyes
Facultad de Ciencias, Instituto de Ciencias Químicas, Isla Teja
Universidad Austral de Chile
Valdivia 5090000, Chile

F. Aiello
National Research Council
Institute for Chemical and Physical Processes (CNR-IPCF)
Via G. Moruzzi 1, Pisa 56124, Italy

F. Balzano, G. Uccello-Barretta
Department of Chemistry and Industrial Chemistry
University of Pisa
via G. Moruzzi 13, Pisa 56124, Italy

J. Rodríguez-Pereira
Center of Materials and Nanotechnologies, Faculty of Chemical
Technology
University of Pardubice
Nam. Cs. Legii 565, Pardubice 53002, Czech Republic

J. Rodríguez-Pereira
Central European Institute of Technology
Brno University of Technology
Purkyňova 123, Brno 612 00, Czech Republic

 The ORCID identification number(s) for the author(s) of this article can be found under <https://doi.org/10.1002/adom.202203096>.

© 2023 The Authors. Advanced Optical Materials published by Wiley-VCH GmbH. This is an open access article under the terms of the Creative Commons Attribution-NonCommercial-NoDerivs License, which permits use and distribution in any medium, provided the original work is properly cited, the use is non-commercial and no modifications or adaptations are made.

DOI: 10.1002/adom.202203096

formation of photoexcited carriers which can be later extracted or emitted in the above technologies,^[15] has opened the door to extend their use, for instance, to perform solar- photo(electro) chemical reactions,^[16–18] using the harvested solar energy to drive chemical reactions. Unfortunately, most practical applications in solar-driven chemistry are performed in polar environments, where the halide perovskite is not long chemically stable enough. At this point, the ionic nature of the PNCs is the main reason to be vulnerable to polar systems, caused by the lability of species coming from the $[\text{PbX}_6]$ octahedra.^[19–21] In this way, a high density of defects can interact with O_2 and polar molecules such as H_2O , promoting the rupture of the halide perovskite crystalline structure.^[22,23] Therefore, non-polar systems are suitable to study the intrinsic properties of the PNCs, maintaining their crystalline integrity.

In this context, recent alternatives such as ligand passivation of PNCs with some robust ligands such as sulfobetaines,^[24–26] lecithin,^[27] aminoacids,^[28,29] bidentate species,^[30] alkylphosphines,^[31,32] among others, can replace conventional oleic acid (OA) and oleylamine (OLA) to increase the PL properties and air-stability of the PNCs.^[33] Even though these ligands can solve the actual drawbacks related to the structural instability of the PNCs, it seems that they are not hydrophobic enough to avoid the material degradation. This fact makes that ligand surface modification to produce highly stable PNCs in polar environments is not a widely exploited topic, yet. Accordingly, promising strategies coming from the material encapsulation through the introduction of polymeric matrices are emerging,^[34] as well as the partial/full coating with inorganic matrices like SiO_2 shells.^[35,36] By employing polysalt ligands composed by quaternary ammonium or imidazolium bromide species, alcohol-stable CsPbBr_3 PNCs can be formed, keeping stable their photophysical features for more than 8 months, taking advantage of the multi-coordination ability from the capping agents in combination with polymeric agents like poly(isobutylene-alt-maleic anhydride) to fill surface defects.^[37] On the other hand, by triggering chemical cross-linkages of OA and OLA ligands to methacrylate-functionalized matrices, MAPbBr_3 PNCs can be stable in extreme organic and aqueous polar systems for 600 days, keeping a PLQY $\approx 70\%$.^[38] In this case, a low concentration of H_2O molecules can penetrate the polymeric matrix to passivate the Br^- deficiency in the perovskite, suppressing the emergence of non-radiative recombination traps.

Alternatively, PNCs and mesoporous SiO_2 composites can be prepared in the presence of stoichiometric amounts of molten salts such as NaNO_3 , KNO_3 , and KBr under ambient conditions and high temperatures $\approx 350^\circ\text{C}$. Composites delivered PLQY higher than 89%, keeping their luminescent properties for 3 h at 180°C , 1 month in both water and aqua regia systems, and 24 h in saline water at 90°C .^[39,40] In this context, ionic species such as K^+ and Br^- are well known to conduct efficient defect passivation by filling A-site and halide-positions in the perovskite structure.^[41] Although the above strategies can ensure the protection of the PNCs from polar solvent interactions, there are some drawbacks to be addressed: i) a high density of ligands covering the PNCs, or the formation of a thick oxide shell restrains the carrier transport into the photomaterial and ii) most of the in situ or post-synthetic treatments have been

employed to stabilize bromine-based PNCs, which show a poor but reasonable inherent stability in polar media. This reflects that a suitable stabilization approach of more sensitive perovskites as the case of narrower band gap iodine-based PNCs is still far away to be developed, becoming more attractive to get a final perovskite with high PL properties, low density of defects, and long-term stable in polar solvents.

In this journey, a didodecyldimethylammonium bromide (DDAB) salt has emerged as an interesting capping ligand providing enhanced carrier transfer and increased stability of PNCs.^[42,43] Although the DDAX ($X = \text{Cl}, \text{Br}$) family has been widely reported to increase the performance of LEDs, enhance luminescent features, and prolong the stability of PNCs in low/high polar mixture systems,^[44] the potential of this capping ligand has not been fully unlocked. Thus, the understanding of the protection mechanism offered by the ligand passivation is limited, being this knowledge key to provide a general protocol to stabilize all type of halide PNCs beyond non-polar media.

Herein, we report for first time the preparation of ultrastable non-encapsulated CsPbX_3 PNCs dispersed in fully alcohol media through a simple and efficient ligand passivation process by action of DDAB. First, we analyzed the role of DDAB concentration on the morphology, structural, PL properties, and surface chemical environment of CsPbBr_3 PNCs. These nanocrystals show a long-term stability in methanol/butanol (MeOH/BuOH) systems around 7 months, reaching an enhanced optical performance. Beyond the filling/replacement of surface defects, DDAB also restrains the full permeation of alcohol to be in contact with the perovskite. At this point, alcohol molecules in form of ionized species can permeate through the ligand layer to remove structural defects. Then, we stabilize air-sensitive $\text{CsPbBr}_{3-x}\text{I}_x$ and CsPbI_3 PNCs in the alcohol environment, showing high PL performance and extended stability up to 6 h of exposure to the polar medium. This contribution offers facile approach to stabilize CsPbX_3 PNCs in polar environments and provides an advance in the development of strategies for PNCs processing and surface ligand engineering.

2. Results and Discussion

To provide a first view about the role of the DDAB on the stability of CsPbBr_3 PNCs in alcohol solvents, Transmission Electron Microscopy (TEM) and Scanning Electron Microscopy (SEM) measurements were performed. First, we combined the PNCs colloidal solutions in hexane with different DDAB concentrations contained in BuOH : 4.3, 8.5, 17, 43, and 85 mM. For TEM analysis, these resultant dispersions (named hereafter as PNCs-BuOH) were analyzed in three different scenarios: i) fresh PNCs-BuOH samples at 0 h in absence of MeOH, ii) 48 h, and iii) 5040 h after adding 600 μL MeOH to the PNCs-BuOH dispersions (we defined these time scenarios as aging times). **Figure 1** and **Figure S1**, Supporting Information show the TEM images of the PNCs dispersed in alcohol medium with and without DDAB at different aging times. For PNCs-BuOH dispersions at 0 day (**Figure 1A–F**), the characteristic nanocube morphology with a particle size between 8.8 and 10 nm is observed. Particle size distribution at different aging

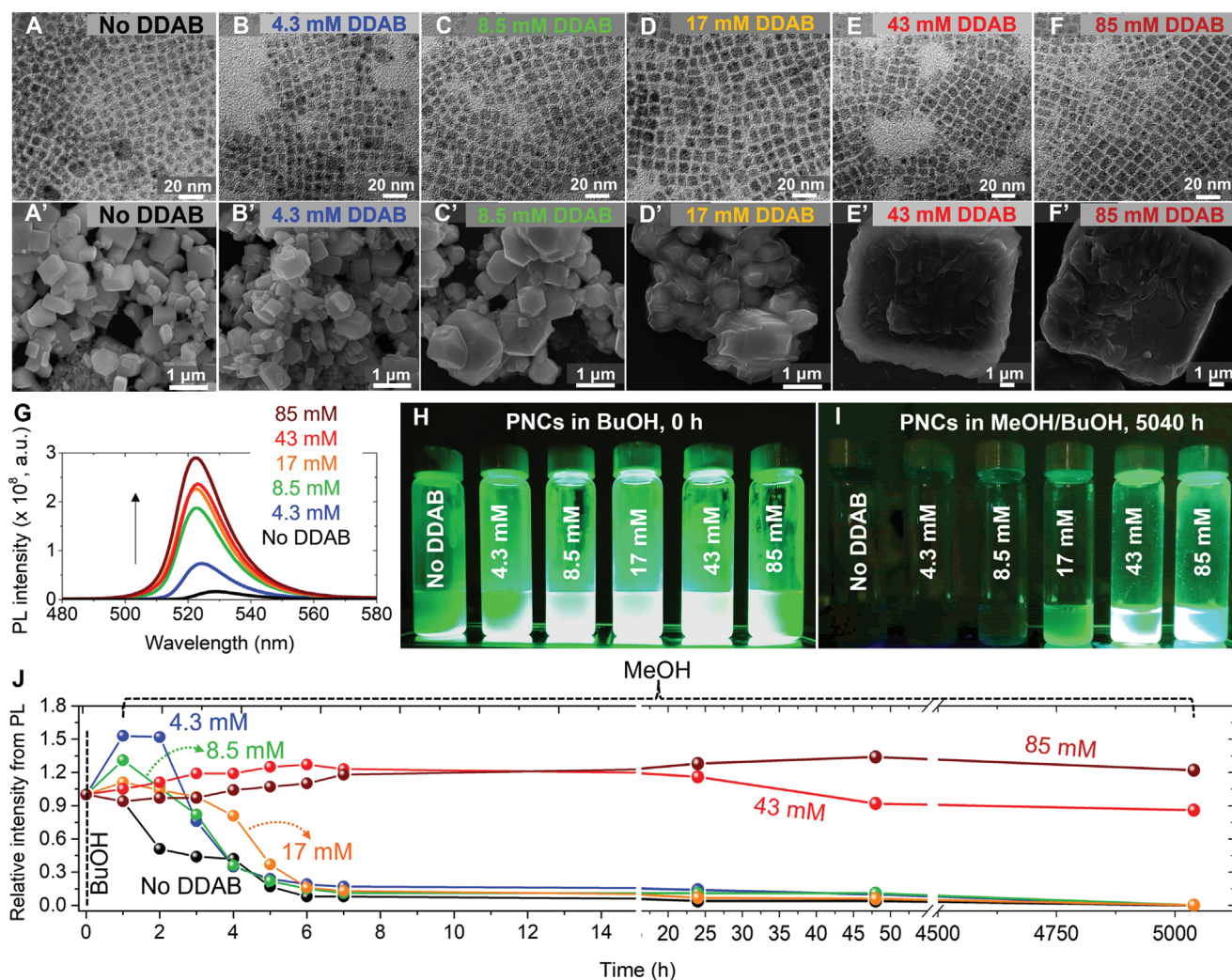


Figure 1. TEM images of CsPbBr₃ PNCs dispersed in A–F) BuOH at 0 h and A'–F') MeOH/BuOH system after 5040 h of aging, in (A, A') absence of DDAB, and in presence of (B, B') 4.3 mM, (C, C') 8.5 mM, (D, D') 17 mM, (E, E') 43 mM, and (F, F') 85 mM DDAB. G) PL spectra, and photographs of green luminescent PNCs dispersed in H) BuOH at 0 h and I) MeOH/BuOH system after 5040 h of aging by varying the DDAB concentration. J) Relative PL intensity of PNCs dispersed in BuOH and MeOH/BuOH systems, by varying the aging time in absence and presence of different DDAB concentrations, see also Figure S5, Supporting Information.

times is summarized in Figure S2, Supporting Information. Selected area diffraction (SAED) measurements (see Figure S3, Supporting Information) corroborate the orthorhombic crystal phase (ICSD 97851) in all the PNCs-BuOH dispersions.^[45] Moreover, the PNCs size for fresh samples is similar up to DDAB concentration of 17 mM, but a slight increase of nanocube size with a better monodispersity is observed at higher DDAB content. The energy dispersive spectroscopy (EDS) (see Table S1, Supporting Information) analysis shows more bromine with higher DDAB concentrations. This evidence suggests that Br coming from the ligand is incorporated in the PNCs structure, indicative of surface passivation.^[46]

After adding MeOH into the PNCs-BuOH dispersions with different DDAB content and aging them for 48 h (see Figure S1, Supporting Information) some changes have been identified. Alcohols such as MeOH promote the removal of carboxyl acid/alkylamine ligands from the CsPbBr₃ surface,^[47] and

a high density of defects is formed, thus increasing the surface energy. Therefore, nanoparticle aggregation and/or the formation of dangling bond are favored to fill the defects.^[48] Consequently, in these conditions pristine CsPbBr₃ exhibits bigger cubes (see Figure S1A, Supporting Information) preserving the crystalline structure (see Figure S3, Supporting Information). Nevertheless, at higher DDAB concentrations, the emergence of large particles is eventually restrained, and an eventual decrease in the particle size is observed (see Figure S1B–F, Supporting Information). At this point, it is reported that DDAB can mediate the partial exfoliation of [PbBr₆]⁴⁻ units from the 3D structure, which favors the Cs⁺ replacement by DDA⁺ cations and hinder the nanocrystals growth.^[49] Accordingly, we deduce that DDAB also partially exfoliates the surface of PNCs in the fresh PNCs-BuOH samples at 0 h, producing small nanoparticles to promote their coalescence and a slight increase of average particle size. However, after 48 h of exposure to the

polar environment, DDAB delays the emergence of bigger nanoparticles, giving an idea about the protective effect of this ligand against the alcohol medium.

Complementarily, SEM images of samples after 5040 h (7 months) in MeOH/BuOH dispersion (Figure 1A'–F'), show particles of the order of microns. This suggests that MeOH can progressively access to the perovskite structure, causing the material agglomeration. In this case, we believe that small-size exfoliated PNCs aggregate to produce microcrystals, being protected by DDAB to avoid/prevent the full alcohol permeation. Accordingly, we conclude that at concentrations of DDAB higher than 17 mM, we can produce an effective passivation layer to restrain the mobility of alcohol species toward PNCs, maintaining their crystalline structure.

The influence of DDAB on the intrinsic properties of PNCs in alcohol systems was also studied through changes in their PL emission. In absence of DDAB, PNCs dispersed in BuOH show a PL signal located at ≈ 530 nm, with an attenuated emission. By contrast, a blueshift in the PL peak position was observed in the presence of a higher DDAB concentration, with higher emission intensity (see Figure 1G). This shift was also reflected in the UV–Vis spectra of PNCs samples, as shown in Figure S4A, Supporting Information. We attribute this optical behavior to the decrease in PNCs particle size caused by the presence of DDAB. As discussed above, DDAB can exfoliate the PNCs surface, generating small nanoparticles and strengthening the quantum confinement effect. Then, the appearance of a low-intense PL peak position for pristine PNCs at longer wavelengths is characteristic of aggregated nanoparticles, facilitating the nonradiative recombination mechanism.^[42] However, the addition of DDAB not only provides more uniformity to the particle size distribution, but also fixes the damaged PNCs surface stoichiometry. This explains why DDAB-capped PNCs give ≈ 1 -order magnitude more emission compared to pristine PNCs, as a result of reduced nonradiative recombination.^[43]

On the other hand, PL measurements as a function of aging time were conducted for all PNCs-BuOH dispersions in presence of MeOH to analyze the optical performance of nanocrystals in a harsher polar medium. Here, PL spectra of PNCs-BuOH dispersions were acquired at 0 and 1 h without MeOH. Later, controlled volumes of MeOH were added to PNCs-BuOH dispersions from 2 to 6 h (at times intervals of 1 h) to reach a total added volume of 600 μ L of MeOH. At this point, the resultant dispersions were aged at different times to reach a maximum of 5040 h. Thus, PL emission of the samples with MeOH was obtained from 2–5040 h (Figure S5, Supporting Information). As observed in Figure 1H,I, we evidenced the effect of the DDAB concentration on green luminescence of PNCs along the time, monitoring some changes in the absorption (see Figure S4B–D, Supporting Information; PL, Figure S5, Supporting Information and the relative emission intensity, and Figure 1J). For pristine PNCs, the PL intensity started to decrease after 1 h in BuOH, and totally quenched after 2 h by adding MeOH. This is associated to the loss of OA/OLA in the alcohol media, and the loss of the emission.^[50] Meanwhile, an increase of the PL of PNCs-BuOH is reached after 1 h at concentrations lower than 17 mM, but this emission is then decreased after MeOH addition, together with a slight redshift in the PL peak position. Compared to MeOH, the longer

hydrocarbon chain can hinder the facile access to PNCs. Nevertheless, a smaller molecule as MeOH can interact with PNCs if the DDAB concentration is low enough to entirely cover the material surface. We confirmed this hypothesis by measuring the PL behavior from the PNCs-BuOH dispersion with the lowest DDAB content, 4.3 mM, evidencing that the PL emission of the material is mainly preserved (see Figure S6, Supporting Information). However, PNCs still present emission after 48 h into the MeOH/BuOH system, concluding that even a low DDAB concentration hinders the total suppression of radiative channels. This fact agrees with the UV–Vis spectra of samples, where the absorption edge of PNCs in presence of DDAB is almost unchanged with the aging time. In this context, DDAB delays the fast material deterioration, which avoids the total suppression of radiative channels in the PNCs structure.

At concentrations higher than 17 mM, a continuous increase of the PL is achieved, deducing that the PL properties of PNCs are enhanced. Surprisingly, the absorption edge, PL features, and relative intensity of perovskite samples at higher DDAB content are preserved after 7 months of aging (see Figure 1J). In addition, a second emission peak at shorter wavelengths (≈ 514 nm) emerges during this period. We ascribed this optical behavior to the formation of microcrystals with different sizes, providing a characteristic PL emission.^[51] The formation of big crystals has also been observed through XRD measurements (see Figure S7, Supporting Information and its associated discussion) by analyzing the corresponding XRD patterns of the PNCs samples dispersed in BuOH and MeOH/BuOH systems by varying the aging time. Then, by continuing increase the DDAB content into the PNCs dispersion, for instance up to 200 mM, PL properties and stability are still preserved (Figure S6B, Supporting Information). This infers that a higher density of DDAB progressively reinforces the surface coverage of the perovskite against the polar environment. Consequently, we can conclude that DDAB can develop an efficient protective effect of the nanocrystals, favoring radiative recombination channel and avoiding the self-degradation in alcohol medium.

With the purpose of studying the chemical composition and environment of the PNCs dispersed in alcohols, X-ray photoelectron spectroscopy (XPS) measurements were conducted. We were able to confirm the presence of C, N, O, Cs, Pb, and Br atoms, see XPS survey spectra in Figure S8, Supporting Information. The corresponding composition of the samples is summarized in Table S2, Supporting Information. **Figure 2A** exhibits the high-resolution (HR) XPS Cs 3d spectra of PNCs-BuOH materials, where a doublet $\approx 724/738$ eV is achieved. These Cs 3d_{5/2} and Cs 3d_{3/2} core levels, respectively, correspond to the existence of Cs⁺ species composing the CsPbBr₃ structure.^[52] On the other hand, typical 3d_{5/2} and 3d_{3/2} core levels located $\approx 68/69$ eV appeared at the HR-XPS Br 3d spectra of the PNCs dispersions (see Figure 2B), associated with Pb–Br bonds from the Cs-(PbBr₆) octahedra.^[53] By comparing the chemical nature of PNCs with and without DDAB, (see Table S2, Supporting Information), Cs⁺ and Br[−] deficiencies in pristine PNCs are evidenced compared to the DDAB-capped PNCs. Thus, pristine PNCs are prone to increase the concentration of defect sites under a poor ligand coverage, compromising their structural integrity and photophysical features. Meanwhile, the DDAB addition preserves the stoichiometry of PNCs, leading

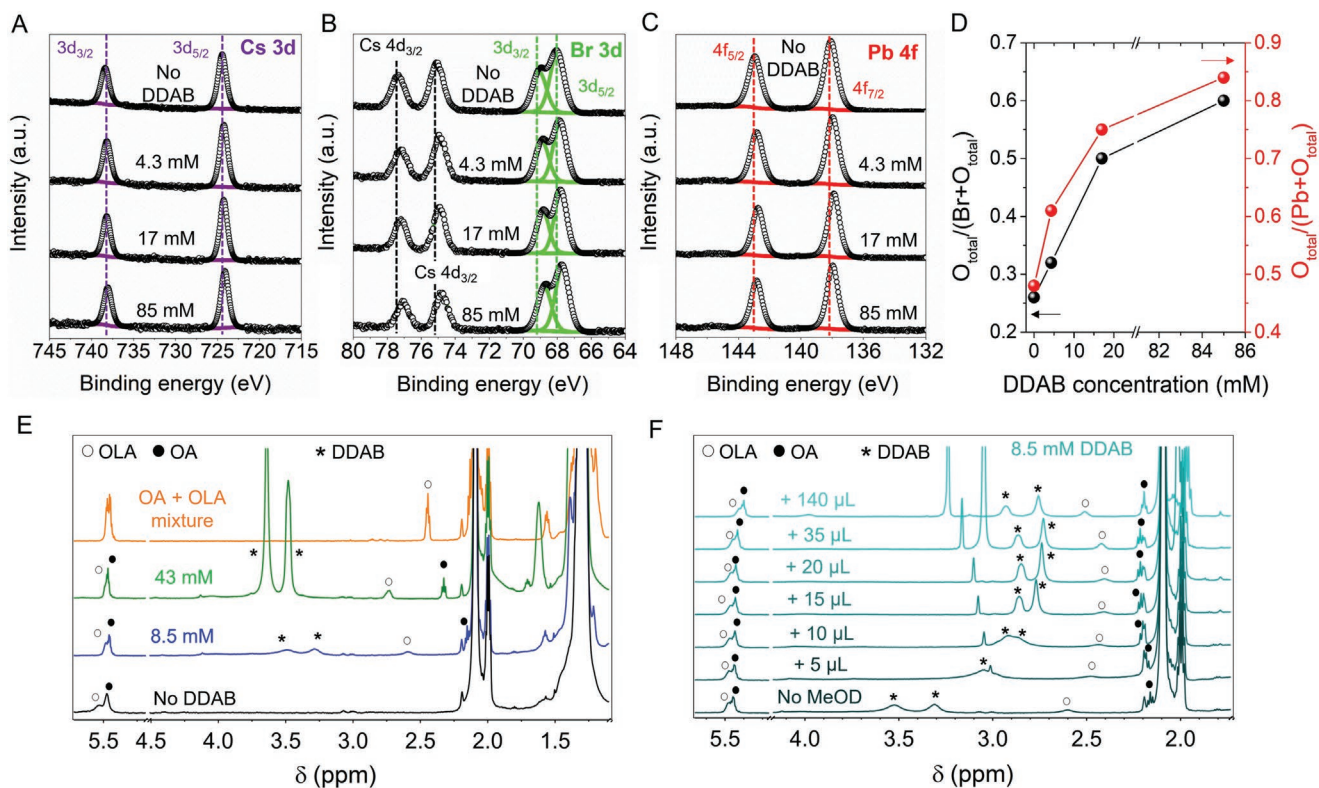


Figure 2. High-resolution XPS A) Cs 3d, B) Br 3d, C) Pb 4f spectra, D) calculated total oxygen-to-halide/total oxygen-to-total lead ratios, and E) ^1H (600 MHz, toluene- d_8 , 298 K) NMR spectra of CsPbBr $_3$ PNCs alone (black) and added by 1 equivalent (blue) or 5 equivalents (green) of DDAB, and equimolar OA/OLA mixture (orange) reported for comparative purposes. F) ^1H (600 MHz, toluene- d_8 , 298 K) NMR spectra of PNCs in presence of 8.5 mM DDAB, titrated with deuterated methanol (MeOD).

to a high optical performance in a polar solvent.^[43,54] This fact corroborates that DDAB impedes the close interaction between alcohol and PNCs avoiding the removal of the ligand shell and the degradation of the PNCs. In addition, the increase of the Br content in presence of DDAB concentration (see Table S2, Supporting Information) suggests that DDAB is an efficient passivation agent to avoid PNCs surface deterioration even in polar media.

Figure 2C shows the HR-XPS Pb 4f spectra of the PNCs-BuOH dispersions, showing the characteristic Pb 4f $_{7/2}$ and Pb 4f $_{5/2}$ core levels \approx 138/143 eV, respectively. This doublet is attributed to the presence of Pb $^{2+}$ species composing the nanocrystal lattice.^[53] Although pristine PNCs exhibit a defective surface by action of the alcohol medium, we did not detect any XPS Pb 4f signals related to the emergence of metallic lead. Since PNCs were washed with MeOAc, this antisolvent removes unreacted species after material synthesis and compensates halide vacancies by binding undercoordinated Pb and COO $^-$ anions.^[55] Then, total oxygen-to-bromine and total oxygen-to-lead ratios [denoted as $O_{\text{total}}/(\text{Br}+O_{\text{total}})$ and $O_{\text{total}}/(\text{Pb}+O_{\text{total}})$] increased upon raising the DDAB concentration (see Figure 2D). This fact suggests that DDAB promotes the oxygen incorporation to the PNCs surface. As seen in Figure S5, Supporting Information, the increased PL intensity of DDAB-capped PNCs in BuOH and after the subsequent MeOH addition evidence that radiative recombination is enhanced due to an effective surface passivation.

With the purpose to identify the interactions between capping ligands and the alcohols, it is pivotal to keep in mind that Cs $^+$ and Pb $^{2+}$ species from PNCs surface are coordinated with oleate anions (OAc $^-$), while halide is linked to oleylammonium (OLAm $^+$) cations.^[7,56] In this context, when small volumes of alcohols such as MeOH, isopropanol, or even H $_2$ O are added into the system, they can partly ionize in their alkyloxonium (R-OH $_2^+$) or/and alkoxide (R-O $^-$) forms mediated by reaction with OA $^-$ and OLAm $^+$, respectively.^[50,57,58] Then, R-OH $_2^+$ and R-O $^-$ can replace some of OA $^-$ and OLAm $^+$ from the PNCs surface. Therefore, we suggest that a higher content of DDA $^+$ cations replacing OLAm $^+$ can produce more ionized species from alkoxides to facilitate the surface coverage, beyond DDAB passivation, filling defect sites of the PNCs and extending their long-term stability.

Although DDAB has been widely used to compensate for the defect sites emerged in the PNCs and improve their intrinsic features, the surface protection mechanism provided by this ligand in polar media such as alcohols has not been elucidated. In order to shed light on surface passivation process of PNCs in alcohol media conducted by DDAB, Nuclear Magnetic Resonance (NMR) spectroscopy analyses were performed, details of the resonance assignment are provided in supporting information.^[59,60] Figure 2E and Figure S9A, Supporting Information show the ^1H NMR spectrum of PNCs dispersed in toluene- d_8 , which was compared with those of pristine ligands (OA+OLA in a molar ratio 1:1), with and without DDAB. We observe that

OLA methylene resonance in α -position with respect to the amine group, which is blended with the baseline when PNCs are dissolved in the deuterated solvent, appears from the baseline as a broad signal centered at $\delta = 2.60$ ppm when one equivalent of DDAB with respect to the estimated OLA content is added. This effect suggests a weakening of the surface interaction, black and blue spectra in Figure S9A, Supporting Information and Figure 2E, which causes a reduction of the signal linewidth. Interestingly, OA methylene resonance in α -position with respect to the carboxyl group is affected as well by DDAB, being shifted till to $\delta = 2.30$ ppm upon addition of the ligand. The resolution and linewidth of such proton signal are comparable to those of the free species, thus pointing out that the acid is not bound to the PNCs surface after DDAB addition (see Figure 2E). Analogously, the olefinic resonances of OA and OLA at $\delta = 5.45$ – 5.47 ppm undergo a variation in shape and position, becoming more similar to the free ligands, especially for OA.

Regarding DDAB, the methylene and methyl protons from its hydrocarbon chains directly bound to the quaternary nitrogen, located at $\delta = 3.45$ and 3.55 ppm, respectively,^[54] are well-resolved in the pure compound and co-presence of OA and OLA ligands has the only consequence of shifting them to lower chemical shifts (see Figure S9A). On the contrary, in the presence of PNCs, a significant increase in DDAB signals' linewidth is detected, as already reported in the literature.^[61] This effect confirms the occurrence of a strong interaction between the surface of the PNCs and DDAB, which causes a slowing down of the additive mobility in solution and, therefore, a complete loss in its signals' resolution. This result, together with the increase of resolution and linewidth observed for the resonances of the capping ligands indicates the favorable ligand exchange process promoted by DDAB, where OLAm^+ and OAc^- ions covering the PNC surface are partly replaced by DDA^+ and Br^- species.^[42]

By increasing DDAB concentration (see Figure 2E and Figure S9B, Supporting Information), the signals belonging to the additive are progressively more consistent to its free species. Additionally, the resonances are shifted at higher frequencies with increasing DDAB concentration. This change is mainly due to changes in DDAB content and ionic strength of the medium, since this behavior has also been observed in DDAB spectra recorded without the perovskite.^[54] At concentrations lower than 8.5 mM, DDAB protons are barely detected as very broad resonances at $\delta = 2.71$ and 2.56 ppm, overlapping with OLA methylene signal (Figure 2E). The additive resonances not only undergo an increase in their linewidth, but they are also more shielded (at the lowest ligand content) if compared to the free compound. It is noteworthy that in the proton spectrum reported in Figure 2E corresponding to a DDAB concentration equal to 8.5 mM, akin to that reported in Figure S9B, Supporting Information, the additive resonances are broader if compared to the latter. We justify this result by taking into account the different sample preparations: in particular, the spectrum in Figure 2E was obtained from a sample prepared by mixing PNCs and DDAB in the minimum amount of solvent required, whereas the spectrum reported in Figure S9B, Supporting Information is obtained by titration.

Deuterated methanol (hereafter named MeOD) was added progressively to PNCs in absence (see Figure S9C, Supporting Information) and presence of DDAB (see Figure 2F). A maximum MeOD volume of 245 and 140 μL was incorporated into the above two systems, respectively, triggering main differences in the surface chemistry of PNCs. The addition of 35 μL of MeOD into pristine PNCs solution causes a shifting of OA signals in the proton spectrum, which are now visible at $\delta = 2.21$ ppm (α - CH_2 ; overlapped with the solvent satellite) and 1.61 ppm (β - CH_2 , Figure S9C, Supporting Information). Signals linewidth of both methylene and olefinic resonances suggests that the ligand is still interacting with the PNCs surface, as well as OLA, given that its methylene resonance is blended with the baseline. The addition of a second portion of alcohol determines an increase of OLA free molar fraction, since its resonance becomes visible at $\delta = 2.48$ ppm, whereas OA signals are better resolved indicating a prevalent free state for this ligand. The fact that OA and OLA resonances become both well resolved when more alcohol is added suggests their detachment from the PNCs surface, because of its material degradation. Conversely, the MeOD dosage to DDAB-capped PNCs remarkably affects the NMR resonances of DDAB rather than the capping ligands. In this case, MeOD was added up to 140 μL , given that this amount is enough to determine degradation in PNCs in the previously discussed titration. When 35 μL are added, (see Figure 2F) DDAB proton signals become more resolved, and the methylene signal, so far located at lower frequencies with respect to the methyl group ($\delta = 3.43$ ppm (CH_3) and 3.52 ppm (CH_2)), is now more deshielded ($\delta = 2.87$ ppm and 2.73 ppm for methylene and methyl groups, respectively). The linewidth of OLA resonance at $\delta = 2.42$ ppm suggests a decrease in the molar fraction bound to the PNCs surface, whereas the resonances belonging to the acid, already free due to DDAB addition, are further deshielded because of the increased polarity.^[54] A more accurate titration in the range 5 – 35 μL was performed, in order to better evaluate the effect of the alcohol on the system. 5 μL of MeOD caused coalescence of DDAB signals that shift at 3.04 ppm, indicating a perturbation of the equilibria in which the additive is involved. The following addition confirms the shift at lower frequencies, and the signals start to differentiate. 15 μL is enough quantity to determine the splitting and the chemical shift inversion of the additive resonances.

This suggests that OLA protons experience only a modest decrease in their line broadening when the titration is performed in the presence of DDAB. Thus, it is likely that the amine moiety stays mainly bound to the PNCs surface even when the amount of alcohol is higher (140 μL). In conclusion, DDAB plays a protective role on polar solvent toward PNCs, preserving the OA and OLA interaction with PNCs surface. We believe that part of OLA molecules released after ligand exchange promotes the formation of alkoxide species, simultaneously producing OLAm^+ which can be linked again to the material surface.

Considering that DDAB has a big influence on the quality and stability of PNCs in full alcohol environment, less defective PNCs with improved and stable photophysical properties can be produced.^[62] Figure 3A exhibits the variation of the PLQY versus time for all the PNCs-BuOH with and without MeOH

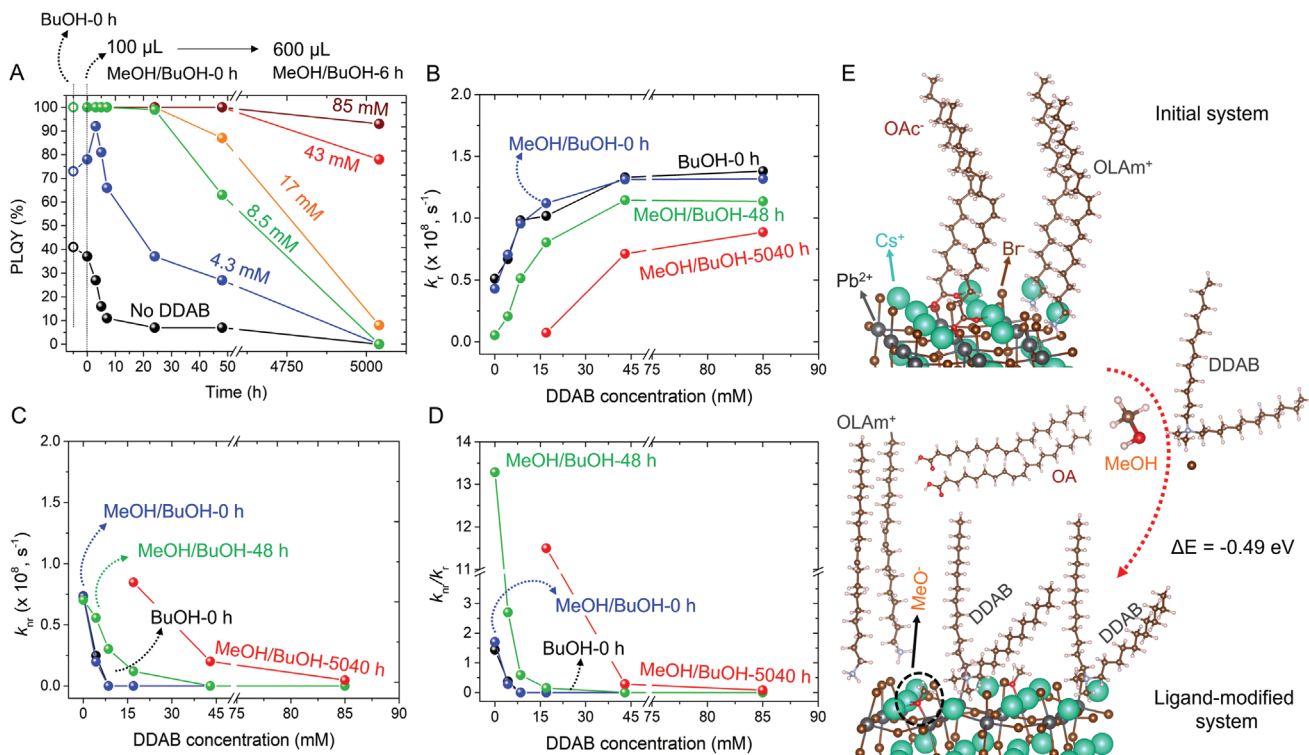


Figure 3. Behavior of A) PLQY, B) radiative (k_r), C) nonradiative recombination (k_{nr}) decay constants, and their D) corresponding k_r/k_{nr} ratio for CsPbBr $_3$ PNCs dispersed in BuOH and MeOH/BuOH systems by varying the aging time in absence and presence of different DDAB concentrations. E) Schematic representation of the ligand passivation of CsPbBr $_3$ PNCs surface conducted by DDAB in presence of MeOH medium. DDA $^+$, OLAm $^+$, Br $^-$ and MeO $^-$ alkoxide species are responsible to produce the protection coverage on perovskite surface.

addition, obtaining the maximum and most stable optical performance at the highest DDAB concentration after 7 months. Here, PLQY of PNCs-BuOH dispersions were acquired at 0 h without MeOH for comparative purposes. Then, controlled volumes of MeOH were added to fresh PNCs-BuOH dispersions from 0 to 6 h (at times intervals of 1 h) to reach a total added volume of 600 μ L of MeOH. At this point, the resultant dispersions were aged at different times to reach a maximum of 5040 h. In this context, PLQY of the samples in presence of MeOH was determined from 0 to 5040 h. As expected, PL features of pristine PNCs are quenched, favoring the formation of non-radiative recombination traps and the alteration of the perovskite lattice. Nevertheless, the progressive enhancement of PLQY to reach values up to 100% indicates that radiative recombination is facilitated with a higher DDAB content. This fact demonstrates that defects sites of PNCs are filled and pure MeOH/BuOH cannot induce degradation on the nanocrystal. As discussed above, the reduction of bromide vacancies and the formation of alkoxide species to interact with Cs-/Pb-rich surface in PNCs generates tolerant-to-defect PNCs in the polar solvent, suppressing the non-radiative recombination.^[50,58] Therefore, at higher DDAB fraction, more DDA $^+$, Br $^-$ and R-O $^-$ species will be available to protect PNCs from alcohol medium. Hence, DDAB concentrations >17 mM ensure that MeOH/BuOH molecules surrounding the DDAB-capped PNCs/polar solvent interface can restrain their diffusion to reach the perovskite, forming enough alkoxide groups to stabilize the materials for long times and produce an enhancement of the

PL properties. Although we have elucidated that higher DDAB concentrations generate a better optical performance and long-term stability in CsPbBr $_3$ PNCs, it is also remarkable that use of these DDAB-capped PNCs as active layers can restrain the operational performance of optoelectronic devices as the case of LEDs. This is because a higher density of the ligand covering the PNCs can act as an insulating layer to hinder the carrier injection/transport into the LEDs. Therefore, future contributions can be focused to establish a suitable DDAB content to simultaneously enhance the PL features of PNCs in polar solvents and allow the fabrication of highly efficient LEDs.

For further insights into how the recombination kinetics of the PNCs samples changes with time, we carried out time-resolved PL measurements at different aging times, in BuOH and MeOH/BuOH systems, as shown in Figure S10, Supporting Information. From each PL decay, we collected the corresponding average electron lifetimes, τ_{avg} , and fitted them through a bi-exponential equation. Although PNCs show a 100% PLQY, their PL dynamics is described by a bi-exponential function. Tables S3–S5, Supporting Information summarize the parameters extracted from the corresponding fitting of PL decays. The bi-exponential behavior has been attributed to the trapping–detrapping phenomenon induced by shallow energy states in the perovskite conduction band (CB) as explained in earlier reports.^[53,63] By adding MeOH and extending the aging time, the τ_{avg} of pristine PNCs was longer. This is associated with the delay of carrier recombination, caused by the generation of halide empty sites controlled by carrier trapping.^[64]

Interestingly, by introducing DDAB, a different PL decay behavior was obtained independently of the aging time. At the lowest DDAB content (4.3 mM), the faster radiative recombination component is lowered (τ_1), while the long-lived radiative contribution increased (τ_2). This suggests that DDAB passivation provides radiative energy levels to PNCs to promote the trapping–detrapping process, facilitating the radiative recombination and increasing the PLQY.^[43]

Similarly, a faster τ_{avg} was observed by increasing the DDAB content, indicating that more radiative channels are present to accelerate the carrier recombination. We believe that the formation of Cs-Br/Pb-Br domains by filling halide vacancies, and the incorporation of oxygen through alkoxide-PNCs surface interaction should introduce shallow donor species to support the radiative recombination dynamics. Then, by contrasting the estimated τ_{avg} for DDAB-capped PNCs in all the time scenarios, it is worth noting that carrier recombination decay is eventually longer, characteristic of bigger perovskite crystals. In this frame, PNCs with DDAB content >17 mM still present PL decay features after 7 months of aging, in line with the microcrystals revealed by SEM (Figure 1D'–F'). Therefore, the first step of DDAB passivation process, surpassing the concentration threshold (17 mM) consists of the formation of PNCs assemblies, generating an effective ligand protection against the permeation of alcohol molecules.

To rationalize the effect of DDAB on the carrier recombination mechanism of PNCs, radiative and nonradiative recombination constants k_r and k_{nr} , respectively, were calculated through PLQY and τ_{avg} values (see Tables S3–S5, Supporting Information). Independently of the time scenarios considered above, the higher the DDAB content in PNCs, the higher the k_r the lower the k_{nr} and k_{nr}/k_r ratios (see Figure 3B–D). This trend can be interpreted considering that the defective PNCs surface is gradually repaired by the inclusion of more Br[−] and oxygenated species, maximizing the suppression of non-radiative channels.^[9,46] In this context, it is evident that the structural exfoliation of PNCs commonly caused by DDAB is minimized, mediating ligand exchange with OLA ligand, key to produce alkoxide ions. Considering that the instability of PNCs in polar solvent is due to the detachment of the long-hydrocarbon chain ligands, mainly OA, Br[−] and oxygenated R-O[−] anions are required to compensate the defective surface of nanocrystals and maintain long-term stability of their intrinsic features. Therefore, we can claim that this is the second step of the DDAB passivation process in alcohol environment.

To gain insight into the mechanism of surface ligand exchange provided by DDAB, we conducted theoretical calculations through density functional theory (DFT), see the SI for further details. We estimated the probability to induce ligand exchange processes of OAc[−] and OLA⁺ species attached to the PNCs surface by DDA⁺, Br[−] and ionized MeOH molecules, represented as MeO[−]. As seen in Figure 3E, the initial system is formed by a CsPbBr₃ slab with four Br vacancies and two Cs vacancies on surface; two of the Br vacancies are occupied by OAc[−] species, Cs⁺ vacancies are occupied by OLA⁺ cations, leaving two free Br deficient sites. When DDAB and MeOH (BuOH) are introduced, the nanocrystal surface is prone to experience the replacement of two Cs⁺ and two Br[−] vacancies by two DDA⁺ and MeO[−] ligands, respectively, while Br[−] species

from DDAB compensate the other free Br defect sites. In this way, two desorbed OA molecules are generated, while two OLA⁺ cations are linked to outer Br atoms.

By computing the total DFT energy difference (ΔE) between initial (I) and ligand-modified (LM) systems (corresponding to the perovskite in absence and presence of DDAB, respectively), we have determined that this surface ligand exchange is thermodynamically favorable, with $\Delta E = -0.49$ eV. Following Figure 3E, $\Delta E = E_{\text{LM}} - E_{\text{I}}$, where E_{LM} is the DFT total energy of the output ligand-modified system, calculated as the sum of the energy of the CsPbBr₃ surface saturated with Br[−] vacancies and ligands DDA⁺, OLA⁺, and MeO[−], plus twice the energy of the isolated OA molecule. On the other hand, E_{I} is the energy of the input initial system, obtained as the sum of the energy of the CsPbBr₃ surface saturated with ligands OAc[−] and OLA⁺, plus twice the energy of the isolated methanol molecule, and twice the energy of the isolated DDAB molecule. This result corroborates the hypothesis established through NMR measurements; the ligand exchange between DDAB and OLA in the presence of alcohols favors the co-emergence of OLA⁺ and alkoxides ions to give an efficient coverage to avoid the damage of PNCs. Then, similar DFT calculations were performed by introducing BuOH instead of MeOH, estimating a higher $\Delta E = -0.33$ eV (see Figure S11, Supporting Information). As expected, the addition of BuOH is energetically more unfavorable, since this organic compound is bigger, and produces larger distortions on the surface. Therefore, we conclude that most of the alkoxide ligands come from MeOH deprotonation to compensate Br deficient sites.

Having elucidated the passivation effect produced by DDAB to trigger a high and stable optical performance in CsPbBr₃ PNCs, we looked for extrapolating this approach to stabilize more sensitive halide PNCs. First, we studied the PL properties of CsPbBr_{3-x}I_x PNCs as a function of time, up to 6 h. These materials were prepared by conducting a halide exchange reaction between DDAB-capped CsPbBr₃ PNCs-BuOH and iodide anions coming from the addition of SrI₂ dissolved in MeOH. Here, stable PNCs-BuOH samples in the presence of 17 and 43 mM DDAB were prepared as starting dispersions. We have chosen these DDAB concentrations due to the stability of CsPbBr₃ PNCs starting to be enhanced into the polar solvents at these values. On the other hand, SrI₂ was chosen as iodine source, since Sr²⁺ species do not easily substitute Pb²⁺ positions into the perovskite structure, guaranteeing that initial chemical nature of the perovskite host is unaltered.^[65] Consequently, only iodide anions would participate in the ion exchange process to obtain mixed halide PNCs (MHPs), leaving Sr as an inert bystander. From the PL spectra shown in Figure 4A,A', we note that the dispersions exhibit distinct anion exchange behavior due to the passivation grade provided by DDAB. Since more Br[−] anions mediate the restoration of the defect sites in Br-PNCs at higher DDAB concentrations, more bromide domains are replaced by iodide anions during the exchange.^[66] Thus, PNCs-BuOH dispersions with high DDAB content require more iodide species to produce a significant redshift in the PL, but the fully exchanged nanocrystals are resistant to alcohol medium even when more MeOH is added. Since the complexation affinity of the Pb–Br bond is higher compared to the Pb–I bond,^[9,66] I[−] anions can migrate out faster from

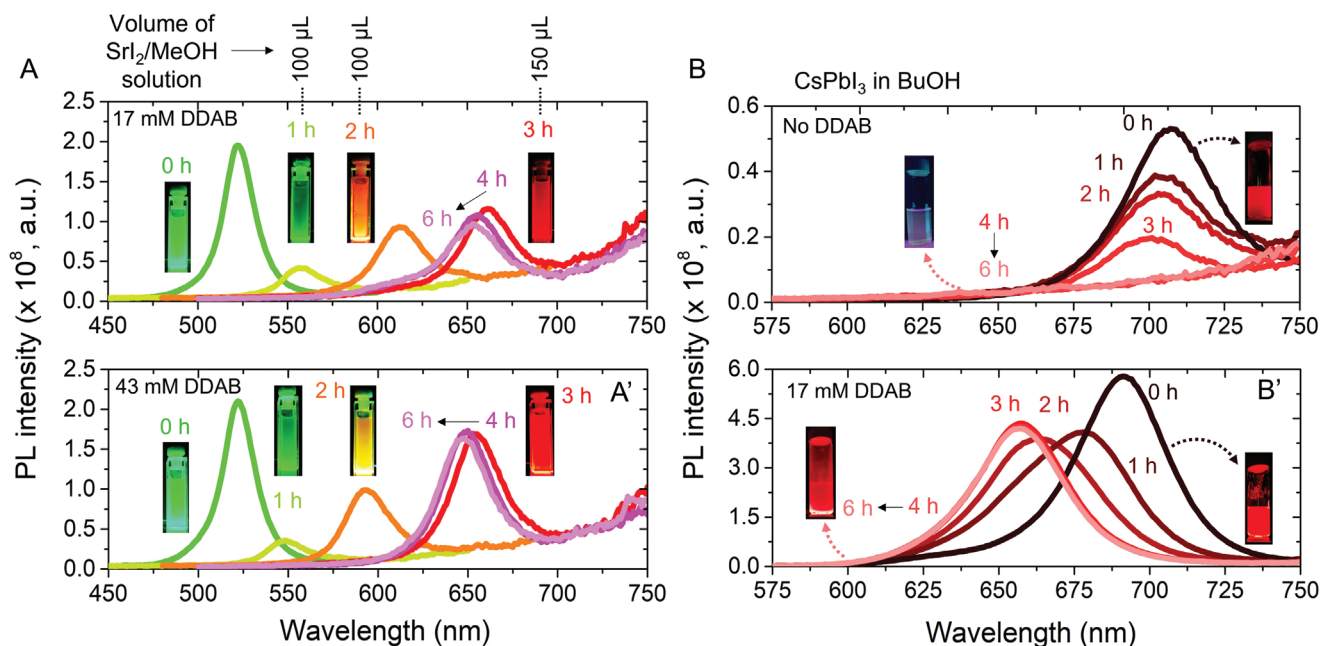


Figure 4. Time-dependent PL spectra of A, A') anion-exchanged $\text{CsPbBr}_{3-x}\text{I}_x$ MHPs dispersed in BuOH at 0 h in presence of A) 17 mM and A') 43 mM DDAB by adding controlled volumes of 200 mg mL^{-1} SrI_2/MeOH solution. Time-dependent PL spectra of B, B') CsPbI_3 PNCs dispersed in BuOH at 0 h B) in absence and B') presence of 17 mM DDAB.

the MHPs, making them more susceptible to possess a defective structure. However, our findings show that the PL feature of MHPs is almost preserved, reaching an increased emission intensity. Therefore, DDAB avoids the fast detachment of iodide from the PNCs, suggesting a strong interaction between DDA^+ and I^- species, while the DDAB protection pathway is maintained.

We also analyze the stabilization of pure CsPbI_3 PNCs dispersed into the alcohol media, in presence of 17 mM DDAB. As seen in Figure S12, Supporting Information, lower DDAB concentrations as 8.5 mM generates a fast degradation of the PNCs, losing their intrinsic properties. Meanwhile, higher DDAB concentrations at 43 mM reinforce the protective coverage on the nanocrystals surface, but the initial red PL emission of the perovskite is not preserved. We attributed this change to the fast anion exchange between DDAB and CsPbI_3 PNCs. Hence, 17 mM DDAB ensures the surface restoration/passivation of iodide perovskite without changing its optical features. Unlike CsPbBr_3 and $\text{CsPbBr}_{3-x}\text{I}_x$ PNCs, the structural integrity of black phase of CsPbI_3 was analyzed in BuOH after 6 h, since this material is rapidly transformed into yellow δ -phase in MeOH, even when DDAB is present. Compared with pristine CsPbI_3 where the PL feature is completely quenched, (see Figure 4B) DDAB-capped CsPbI_3 PNCs are still luminescent exhibiting a slight blueshift in the PL peak position (Figure 4B'). This is due to the Br^- passivation of halide defects generated by the gradual iodide migration.^[46] It is clear that a low concentration of DDAB does not lead to an effective coverage of the iodide-PNCs surface, allowing MeOH molecules to reach the perovskite, promoting the diffusion of a high iodide fraction to the polar solvent, and causing the octahedral distortion. Nevertheless, DDAB can delay the access of bigger alcohol molecules such as BuOH, making an in situ halide compensation in the PNCs.

We believe that DDAB passivation is an interesting option to supply surface defect centers, both to generate a protective shell against full permeation of alcohols and to prepare more stable CsPbX_3 PNCs in polar solvents. In summary, DDAB passivation can be considered as a simply alternative to repair the PNCs surface, providing an efficient ligand coverage, and producing stable dispersions, which could be beneficial for future developments in optoelectronics and solar-driven reactions in polar media.

3. Conclusions

In this work, we introduce ligand passivation as a promising strategy to prepare highly stable CsPbX_3 PNCs in full alcohol environments, with a tolerant-to-defect structure and improved optical performance. By introducing DDAB ligand, a suitable surface coverage of the PNCs was achieved, being more effective at higher concentrations. We elucidated that a two-step passivation mechanism dictates the long-term stability of PNCs: i) formation of nanocrystals aggregates protected by DDAB to hinder the permeation of alcohol molecules, and ii) the restoration of the surface stoichiometry to decrease the density of halide deficient sites. By understanding that PL properties of OA/OLA-capped PNCs are quenched by the fast ligand detachment in the presence of alcohols to compromise the structural integrity of materials, DDAB generates a partial ligand exchange with the native capping ligands to generate both more Cs-Br/Pb-Br domains and the incorporation of oxygen to interact with the Cs-/Pb-rich surface sites. We deduce that part of OLA released during the ligand exchange process can partly ionize the alcohol species to produce alkoxide anions, which together with Br^- species, enhance the radiative recombination

pathway and suppresses the non-radiative carrier traps. Consequently, we were able to produce high-quality CsPbBr₃ PNCs alcohol dispersions with PLQY of up to 100% and stability up to 7 months. We extrapolated this strategy to stabilize CsPbBr_{3-x}I_x and CsPbI₃ PNCs, realizing that DDAB delays the iodide diffusion toward the polar solvent, and favor the in situ compensation of iodide deficiency during halide loss. Thus, it is possible to extend the PL emission and stability of these iodide-PNCs up to 6 h in the alcohol media, delaying the deterioration of the optical features. This work offers a simple way to prepare highly resistant multicolor CsPbX₃ dispersions, suitable for conducting future contributions in optoelectronics and solar-driven chemical applications in polar media. Current efforts should be focused on the incorporation of iodide-based capping ligands, where a suitable concentration would maximize the resistance of CsPbI₃ PNCs in polar solvents, including MeOH.

Supporting Information

Supporting Information is available from the Wiley Online Library or from the author.

Acknowledgements

This work was supported by the European Innovation Council (EIC) via OHPERA project (grant agreement 101071010), the Spanish Ministry of Science and Innovation under projects STABLE (PID2019-107314RB-I00) and ECOCAT (PID2020-116093RB-C41), the Spanish Ministry of Science and Innovation under project She-LED (PID2021-122960OA-I00), and the Generalitat Valenciana via Prometeo Grant Q-Solutions (CIPROM/2021/078). C.A.M. acknowledges APOSTD grant (APOSTD/2021/251) for funding. The authors also thank the Ministry of Education, Youth and Sports of the Czech Republic for the financial support of XPS measurements using CEMNAT infrastructure (project LM 2018103). The authors are very grateful to the “Serveis Centrals d’Instrumentació Científica (SCIC)” of the Universitat Jaume I.

Conflict of Interest

The authors declare no conflict of interest.

Author Contributions

A.F.G.-R., S.M., S.G. and I.M.-S. conceived the project. A.F.G.-R., R.F.-C., S.M., S.G. and C.A.M. designed the experiments. A.F.G.-R. synthesized PNCs colloidal solutions and films, and performed the corresponding morphological, structural, and optical properties. C.E.-A. performed the theoretical calculations. J.R.-P. contributed to the XPS measurements and analysis. S.M., F.A., F.B., and G.U.-B. designed and performed the NMR analysis. A.F.G.-R. and C.A.M. coordinated the experimental work. A.F.G.-R. and I.M.-S. coordinated the whole project. All authors contributed to the discussions and the writing of the manuscript.

Data Availability Statement

The data that support the findings of this study are available from the corresponding author upon reasonable request.

Keywords

halide perovskites, photocatalysis, photoluminescence quantum yield, polar solvents, stability

Received: December 24, 2022

Revised: February 5, 2023

Published online:

- [1] L. C. Schmidt, A. Pertegás, S. González-Carrero, O. Malinkiewicz, S. Agouram, G. Mínguez Espallargas, H. J. Bolink, R. E. Galian, J. Pérez-Prieto, *J. Am. Chem. Soc.* **2014**, *136*, 850.
- [2] L. Protesescu, S. Yakunin, M. I. Bodnarchuk, F. Krieg, R. Caputo, C. H. Hendon, R. X. Yang, A. Walsh, M. V. Kovalenko, *Nano Lett.* **2015**, *15*, 3692.
- [3] E. Scharf, F. Krieg, O. Elimelech, M. Oded, A. Levi, D. N. Dirin, M. V. Kovalenko, U. Banin, *Nano Lett.* **2022**, *22*, 4340.
- [4] M. Vallés-Pelarda, A. F. Gualdrón-Reyes, C. Felip-León, C. A. Angulo-Pachón, S. Agouram, V. Muñoz-Sanjose, J. F. Miravet, F. Galindo, I. Mora-Seró, *Adv. Opt. Mater.* **2021**, *9*, 2001786.
- [5] E. M. Sanehira, A. R. Marshall, J. A. Christians, S. P. Harvey, P. N. Ciesielski, L. M. Wheeler, P. Schulz, L. Y. Lin, M. C. Beard, J. M. Luther, *Sci. Adv.* **2017**, *3*, eaao4204.
- [6] N. Pradhan, *J. Phys. Chem. Lett.* **2019**, *10*, 5847.
- [7] A. Dutta, S. K. Dutta, S. Das Adhikari, N. Pradhan, *ACS Energy Lett.* **2018**, *3*, 329.
- [8] J.-S. Yao, J. Ge, K.-H. Wang, G. Zhang, B.-S. Zhu, C. Chen, Q. Zhang, Y. Luo, S.-H. Yu, H.-B. Yao, *J. Am. Chem. Soc.* **2019**, *141*, 2069.
- [9] A. F. Gualdrón-Reyes, S. Masi, I. Mora-Seró, *Trends Chem.* **2021**, *3*, 499.
- [10] Y.-H. Kim, S. Kim, A. Kakekhani, J. Park, J. Park, Y.-H. Lee, H. Xu, S. Nagane, R. B. Wexler, D.-H. Kim, S. H. Jo, L. Martínez-Sarti, P. Tan, A. Sadhanala, G.-S. Park, Y.-W. Kim, B. Hu, H. J. Bolink, S. Yoo, R. H. Friend, A. M. Rappe, T.-W. Lee, *Nat. Photonics* **2021**, *15*, 148.
- [11] Y.-H. Kim, J. Park, S. Kim, J. S. Kim, H. Xu, S.-H. Jeong, B. Hu, T.-W. Lee, *Nat. Nanotechnol.* **2022**, *17*, 590.
- [12] J. S. Kim, J.-M. Heo, G.-S. Park, S.-J. Woo, C. Cho, H. J. Yun, D.-H. Kim, J. Park, S.-C. Lee, S.-H. Park, E. Yoon, N. C. Greenham, T.-W. Lee, *Nature* **2022**, *611*, 688.
- [13] M. Hao, Y. Bai, S. Zeiske, L. Ren, J. Liu, Y. Yuan, N. Zarrabi, N. Cheng, M. Ghasemi, P. Chen, M. Lyu, D. He, J.-H. Yun, Y. Du, Y. Wang, S. Ding, A. Armin, P. Meredith, G. Liu, H.-M. Cheng, L. Wang, *Nat. Energy* **2020**, *5*, 79.
- [14] M. Albaladejo-Siguan, E. C. Baird, D. Becker-Koch, Y. Li, A. L. Rogach, Y. Vaynzof, *Adv. Energy Mater.* **2021**, *11*, 2003457.
- [15] A. Dey, J. Ye, A. De, E. Debroye, S. K. Ha, E. Bladt, A. S. Kshirsagar, Z. Wang, J. Yin, Y. Wang, L. N. Quan, F. Yan, M. Gao, X. Li, J. Shamsi, T. Debnath, M. Cao, M. A. Scheel, S. Kumar, J. A. Steele, M. Gerhard, L. Chouhan, K. Xu, X.-g. Wu, Y. Li, Y. Zhang, A. Dutta, C. Han, I. Vincon, A. L. Rogach, et al., *ACS Nano* **2021**, *15*, 10775.
- [16] M.-Z. Yang, Y.-F. Xu, J.-F. Liao, X.-D. Wang, H.-Y. Chen, D.-B. Kuang, *J. Mater. Chem. A* **2019**, *7*, 5409.
- [17] D. Cardenas-Morcoso, A. F. Gualdrón-Reyes, A. B. Ferreira Vitoreti, M. García-Tecedor, S. J. Yoon, M. Solís de la Fuente, I. Mora-Seró, S. Gimenez, *J. Phys. Chem. Lett.* **2019**, *10*, 630.
- [18] R. Tang, L. Wang, Z. Zhang, W. Yang, H. Xu, A. Kheradmand, Y. Jiang, R. Zheng, J. Huang, *Appl. Catal., B* **2021**, *296*, 120382.
- [19] H. Huang, B. Pradhan, J. Hofkens, M. B. J. Roeffaers, J. A. Steele, *ACS Energy Lett.* **2020**, *5*, 1107.
- [20] J.-K. Sun, S. Huang, X.-Z. Liu, Q. Xu, Q.-H. Zhang, W.-J. Jiang, D.-J. Xue, J.-C. Xu, J.-Y. Ma, J. Ding, Q.-Q. Ge, L. Gu, X.-H. Fang, H.-Z. Zhong, J.-S. Hu, L.-J. Wan, *J. Am. Chem. Soc.* **2018**, *140*, 11705.

- [21] N. Aristidou, I. Sanchez-Molina, T. Chotchuangchuchaval, M. Brown, L. Martinez, T. Rath, S. A. Haque, *Angew. Chem.* **2015**, *127*, 8326.
- [22] B. Murali, S. Dey, A. L. Abdelhady, W. Peng, E. Alarousu, A. R. Kirmani, N. Cho, S. P. Sarmah, M. R. Parida, M. I. Saidaminov, A. A. Zhumekenov, J. Sun, M. S. Alias, E. Yengel, B. S. Ooi, A. Amassian, O. M. Bakr, O. F. Mohammed, *ACS Energy Lett.* **2016**, *1*, 1119.
- [23] E. Mosconi, J. M. Aspiroz, F. De Angelis, *Chem. Mater.* **2015**, *27*, 4885.
- [24] F. Krieg, S. T. Ochsenbein, S. Yakunin, S. ten Brinck, P. Aellen, A. Süess, B. Clerc, D. Guggisberg, O. Nazarenko, Y. Shynkarenko, S. Kumar, C.-J. Shih, I. Infante, M. V. Kovalenko, *ACS Energy Lett.* **2018**, *3*, 641.
- [25] R. Grisorio, F. Fasulo, A. B. Muñoz-García, M. Pavone, D. Conelli, E. Fanizza, M. Striccoli, I. Allegretta, R. Terzano, N. Margiotta, P. Vivo, G. P. Suranna, *Nano Lett.* **2022**, *22*, 4437.
- [26] F. Krieg, P. C. Sercel, M. Burian, H. Andrusiv, M. I. Bodnarchuk, T. Stöferle, R. F. Mahrt, D. Naumenko, H. Amenitsch, G. Rainò, M. V. Kovalenko, *ACS Cent. Sci.* **2020**, *7*, 135.
- [27] F. Krieg, Q. K. Ong, M. Burian, G. Rainò, D. Naumenko, H. Amenitsch, A. Süess, M. J. Grotevent, F. Krumeich, M. I. Bodnarchuk, I. Shorubalko, F. Stellacci, M. V. Kovalenko, *J. Am. Chem. Soc.* **2019**, *141*, 19839.
- [28] S. Ghosh, P. Kar, *Inorg. Chem.* **2022**, *61*, 10079.
- [29] D. Jia, J. Chen, M. Yu, J. Liu, E. M. J. Johansson, A. Hagfeldt, X. Zhang, *Small* **2020**, *16*, 2001772.
- [30] Y. Li, M. Cai, M. Shen, Y. Cai, R.-J. Xie, *J. Mater. Chem. C* **2022**, *10*, 8356.
- [31] K.-H. Peng, S.-H. Yang, Z.-Y. Wu, H.-C. Hsu, *ACS Omega* **2021**, *6*, 10437.
- [32] F. Liu, Y. Zhang, C. Ding, S. Kobayashi, T. Izuishi, N. Nakazawa, T. Toyoda, T. Ohta, S. Hayase, T. Minemoto, K. Yoshino, S. Dai, Q. Shen, *ACS Nano* **2017**, *11*, 10373.
- [33] A. F. Gualdrón-Reyes, C. A. Mesa, S. Giménez, I. Mora-Seró, *Sol. RRL* **2022**, *6*, 2200012.
- [34] J. Zhu, Z. Xie, X. Sun, S. Zhang, G. Pan, Y. Zhu, B. Dong, X. Bai, H. Zhang, H. Song, *ChemNanoMat* **2018**, *5*, 346.
- [35] Y. Jing, M. J. M. Merckx, J. Cai, K. Cao, W. M. M. Kessels, A. J. M. Mackus, R. Chen, *ACS Appl. Mater. Interfaces* **2020**, *12*, 53519.
- [36] Z. Zheng, L. Liu, F. Yi, J. Zhao, *J. Lumin.* **2019**, *216*, 116722.
- [37] S. Wang, L. Du, S. Donmez, Y. Xin, H. Mattoussi, *Nanoscale* **2021**, *13*, 16705.
- [38] J. Jang, Y. H. Kim, S. Park, D. Yoo, H. Cho, J. Jang, H. B. Jeong, H. Lee, J. M. Yuk, C. B. Park, D. Y. Jeon, Y. H. Kim, B. S. Bae, T. W. Lee, *Adv. Mater.* **2020**, *33*, 2005255.
- [39] M. N. An, S. Park, R. Brescia, M. Lutfullin, L. Sinatra, O. M. Bakr, L. De Trizio, L. Manna, *ACS Energy Lett.* **2021**, *6*, 900.
- [40] Z. Liu, L. Sinatra, M. Lutfullin, Y. P. Ivanov, G. Divitini, L. De Trizio, L. Manna, *Adv. Energy Mater.* **2022**, *12*, 2201948.
- [41] M. Abdi-Jalebi, Z. Andaji-Garmaroudi, S. Cacovich, C. Stavrakas, B. Philippe, J. M. Richter, M. Alsari, E. P. Booker, E. M. Hutter, A. J. Pearson, S. Lilliu, T. J. Savenije, H. Rensmo, G. Divitini, C. Ducati, R. H. Friend, S. D. Stranks, *Nature* **2018**, *555*, 497.
- [42] L. J. Ruan, B. Tang, Y. Ma, *J. Phys. Chem. C* **2019**, *123*, 11959.
- [43] M. I. Bodnarchuk, S. C. Boehme, S. ten Brinck, C. Bernasconi, Y. Shynkarenko, F. Krieg, R. Widmer, B. Aeschlimann, D. Günther, M. V. Kovalenko, I. Infante, *ACS Energy Lett.* **2018**, *4*, 63.
- [44] Y. Shynkarenko, M. I. Bodnarchuk, C. Bernasconi, Y. Berezovska, V. Verteletskyi, S. T. Ochsenbein, M. V. Kovalenko, *ACS Energy Lett.* **2019**, *4*, 2703.
- [45] J. Liu, K. Song, Y. Shin, X. Liu, J. Chen, K. X. Yao, J. Pan, C. Yang, J. Yin, L.-J. Xu, H. Yang, A. M. El-Zohry, B. Xin, S. Mitra, M. N. Hedhili, I. S. Roqan, O. F. Mohammed, Y. Han, O. M. Bakr, *Chem. Mater.* **2019**, *31*, 6642.
- [46] Y. Huang, W. Luan, M. Liu, L. Turyanska, *J. Mater. Chem. C* **2020**, *8*, 2381.
- [47] Y. Sun, H. Zhang, K. Zhu, W. Ye, L. She, X. Gao, W. Ji, Q. Zeng, *RSC Adv.* **2021**, *11*, 27333.
- [48] J. Chen, X. Huang, Z. Xu, Y. Chi, *ACS Appl. Mater. Interfaces* **2022**, *14*, 33703.
- [49] S. K. Balakrishnan, P. V. Kamat, *Chem. Mater.* **2017**, *30*, 74.
- [50] X. Liu, Z. Luo, W. Yin, A. P. Litvin, A. V. Baranov, J. Zhang, W. Liu, X. Zhang, W. Zheng, *Nanoscale Adv.* **2020**, *2*, 2.
- [51] D. Baranov, A. Fieramosca, R. X. Yang, L. Polimeno, G. Lerario, S. Toso, C. Giansante, M. D. Giorgi, L. Z. Tan, D. Sanvitto, L. Manna, *ACS Nano* **2020**, *15*, 650.
- [52] M. Deepa, M. Salado, L. Calio, S. Kazim, S. M. Shivaprasad, S. Ahmad, *Phys. Chem. Chem. Phys.* **2017**, *19*, 4069.
- [53] C. Lee, Y. Shin, A. Villanueva-Antoli, S. Das Adhikari, J. Rodríguez-Pereira, J. M. Macak, C. Mesa, S. J. Yoon, A. F. Gualdrón-Reyes, I. M. Seró, *Chem. Mater.* **2021**, *33*, 8745.
- [54] M. Imran, P. Ijaz, L. Goldoni, D. Maggioni, U. Petralanda, M. Prato, G. Almeida, I. Infante, L. Manna, *ACS Energy Lett.* **2019**, *4*, 819.
- [55] R. Han, Q. Zhao, J. Su, X. Zhou, X. Ye, X. Liang, J. Li, H. Cai, J. Ni, J. Zhang, *J. Phys. Chem. C* **2021**, *125*, 8469.
- [56] Y. Fu, T. Wu, J. Wang, J. Zhai, M. J. Shearer, Y. Zhao, R. J. Hamers, E. Kan, K. Deng, X. Y. Zhu, S. Jin, *Nano Lett.* **2017**, *17*, 4405.
- [57] F. Fang, W. Chen, Y. Li, H. Liu, M. Mei, R. Zhang, J. Hao, M. Mikita, W. Cao, R. Pan, K. Wang, X. W. Sun, *Adv. Funct. Mater.* **2018**, *28*, 1706000.
- [58] X. Zhang, X. Bai, H. Wu, X. Zhang, C. Sun, Y. Zhang, W. Zhang, W. Zheng, W. W. Yu, A. L. Rogach, *Angew. Chem., Int. Ed.* **2018**, *57*, 3337.
- [59] G. Almeida, L. Goldoni, Q. Akkerman, Z. Dang, A. H. Khan, S. Marras, I. Moreels, L. Manna, *ACS Nano* **2018**, *12*, 1704.
- [60] E. Hassanabadi, M. Latifi, A. F. Gualdrón-Reyes, S. Masi, S. Y. Joon, M. Poyatos, B. Julián-López, I. M. Seró, *Nanoscale* **2020**, *12*, 14194.
- [61] F. Zaccaria, B. Zhang, L. Goldoni, M. Imran, J. Zito, B. van Beek, S. Lauciello, L. De Trizio, L. Manna, I. Infante, *ACS Nano* **2022**, *16*, 1444.
- [62] S. R. Smock, Y. Chen, A. J. Rossini, R. L. Brutchey, *Acc. Chem. Res.* **2021**, *54*, 707.
- [63] V. S. Chirvony, K. S. Sekerbayev, H. Pashaei Adl, I. Suárez, Y. T. Taurbayev, A. F. Gualdrón-Reyes, I. Mora-Seró, J. P. Martínez-Pastor, *J. Lumin.* **2020**, *221*, 117092.
- [64] L. Piveteau, M. Aebli, N. Yazdani, M. Millen, L. Korosec, F. Krieg, B. M. Benin, V. Morad, C. Piveteau, T. Shiroka, A. Comas-Vives, C. Copéret, A. M. Lindenberg, V. Wood, R. Verel, M. V. Kovalenko, *ACS Cent. Sci.* **2020**, *6*, 1138.
- [65] A. F. Gualdrón-Reyes, D. F. Macias-Pinilla, S. Masi, C. Echeverría-Arrondo, S. Agouram, V. Muñoz-Sanjosé, J. Rodríguez-Pereira, J. M. Macak, I. Mora-Seró, *J. Mater. Chem. C* **2021**, *9*, 1555.
- [66] A. F. Gualdrón-Reyes, J. Rodríguez-Pereira, E. Amado-González, J. Rueda-P, R. Ospina, S. Masi, S. J. Yoon, J. Tirado, F. Jaramillo, S. Agouram, V. Muñoz-Sanjosé, S. Giménez, I. Mora-Seró, *ACS Appl. Mater. Interfaces* **2020**, *12*, 914.